Ab initio calculations of free energy of activation at multiple electronic structure levels made affordable: An effective combination of perturbation theory and machine learning

Tomáš Bučko,[*,†,‡] Monika Gešvandtnerová,[†] and Dario Rocca[*,¶]

†*Department of Physical and Theoretical Chemistry, Faculty of Natural Sciences, Comenius University in Bratislava, Ilkovičova 6, SK-84215 Bratislava, Slovakia*

‡*Institute of Inorganic Chemistry, Slovak Academy of Sciences, Dúbravská cesta 9, SK-84236 Bratislava, Slovakia*

¶*Université de Lorraine and CNRS, LPCT UMR 7019, F-54000 Nancy, France.*

E-mail: tomas.bucko@uniba.sk; dario.rocca@univ-lorraine.fr

Abstract

While free energies are fundamental thermodynamic quantities to characterize chemical reactions, their calculation based on ab initio theory is usually limited by the high computational cost. This is particularly true if multiple levels of theory have to be tested to establish their relative accuracy, if highly expensive quantum mechanical approximations are of interest, and also if several different temperatures have to be considered. We present an ab initio approach that effectively couples perturbation theory and machine learning to make ab initio free energy calculations more affordable. Starting from results based on a certain production ab initio theory, perturbation theory is applied to obtain free energies. The large number of single point calculations

required by a brute force application of this approach are here significantly decreased by applying machine learning techniques. Importantly, the training of the machine learning model requires only a small amount of data and does not need to be performed again when the temperature is decreased. The accuracy and efficiency of this method is demonstrated by computing the free energy of activation of the proton exchange reaction in the zeolite chabazite. Starting from an ab initio calculation based on a semilocal approximation of density functional theory, free energies based on significantly more expensive non-local van der Waals and hybrid functionals are obtained with only a few tens of additional single point calculations. In this way this work paves the route to quick free energy calculations using different levels of theory or approximations that would be too computationally expensive to be directly employed in molecular dynamics or Monte Carlo simulations.

1 Introduction

Free energy is certainly one of the most important thermodynamic quantities used to characterize chemical reactions. The knowledge of the free energy of activation ($\Delta A^{\ddagger}$), for instance, allows for a determination of the rate constant via Eyring-Polanyi equation[1]

$$k_{R\to P} = \frac{k_B T}{h} \exp\left(-\frac{\Delta A^{\ddagger}}{k_B T}\right), \tag{1}$$

providing thus an access to reaction kinetics. Similarly, by employing the expression

$$K_{R\to P} = \exp\left(-\frac{\Delta A_{R\to P}}{k_B T}\right), \tag{2}$$

the free energy of reaction ($\Delta A_{R\to P}$) defined as a free energy difference between the product (P) and the reactant (R) states can be used to determine the equilibrium constant ($K_{R\to P}$) expressing the relative proportion of P and R at equilibrium.

The accurate calculation of free energy for chemical transformations is complicated by

the necessity to sample the configuration space between reactant and product, whereby some relevant configurations, especially those close to the transition region, receive Boltzmann weights that are often many orders of magnitude lower than those for configurations of stable states. This fact precludes a direct use of standard molecular dynamics (MD) or Monte Carlo (MC) approaches and therefore specialized simulation techniques, such as umbrella sampling,[2] blue moon ensemble technique,[3] or metadynamics,[4] have to be employed instead. As the use of all these techniques is in itself very time consuming, the systematic comparison of different electronic structure methods to find the best description of a chemical reaction is rarely attempted. Similarly, the use of highly accurate but computationally demanding quantum chemical approximations (e.g. coupled-cluster theory[5]) in free energy calculations is limited by the significant computational requirements. Indeed, an effective design of methods for effective and accurate ab initio free energy calculations is a highly important task that was addressed also in several previous reports where the schemes were proposed to compare stability of various conformers or stable phases of materials at different levels of theory,[6,7] determine chemical potentials of various species,[8] free energies of solvation,[9] or free energy profiles for chemical reactions.[10–14] The machine learning (ML) based algorithms turn out to be a very useful in this respect as they allow for inexpensive calculations of energies of configurations,[6,10,13] acceleration of the configuration space sampling,[7,8,12] or improving the quality of results at the post-processing stage.[11] In this work we focus on calculations of free energy of activation. To this end, we propose an efficient simulation protocol combining concepts from free energy perturbation theory[15] (FEPT) and our recently introduced machine learning thermodynamic perturbation theory (MLPT) method[16] that allows to recompute the free energy difference determined at a certain level of theory (designated hereafter as a production method) at another level of theory (target method). Most importantly, we show that such a calculation can be accomplished by performing only a few tens of extra single point energy calculations at the target method level of theory (possibly including computationally expensive methods for which energy gradients may not

even be available). This is achieved by using a small set of explicit calculations to train a ML algorithm whose predictions provide the data required to reach full convergence. We note that a similar idea has been employed in previous work of Shen[10] but our method differs in several important details that we discuss in Sec. 5. The use of our method is exemplified on the calculation of the free energy of activation for the proton exchange reaction between two oxygen sites in zeolite chabazite (see Fig. 1), which has been investigated in several previous theoretical studies.[17,18] Specifically, starting from a production run based on a numerically efficient semi-local approximation[19] of density functional theory (DFT), the free energy of activation of this reaction is computed using the non-local van der Waals (vdW) functional optPBE-vdW[20–23] and the hybrid functional HSE06.[24–26] The latter two methods are considered to be superior to the former because of different reasons: optPBE-vdW accounts for long range London dispersion interactions, which are not described correctly by the semi-local DFT, while the inclusion of the Hartree-Fock exchange in HSE06 should reduce the well known problem with underestimation of barriers for proton transfer reactions by the generalized gradient approximation to DFT.[27]

Additional numerical properties of this new approach are also analyzed in detail. It is shown that a ML algorithm trained on data from simulations at a certain temperature preserves a high level of accuracy also for lower temperatures. This allows for free energy computations in a wide interval of temperatures without additional expensive target method calculations. It is also demonstrated that our method provides accurate predictions beyond the expected range of applicability: by considering only training energies from reactant and transition state configurations the ML algorithm predicts accurate potential energies (and free energies) also for intermediate points along the reaction path. Finally, by exploiting the high predictive power of our ML model coupled with Monte Carlo sampling, we devise a numerical procedure to correct for the inaccuracies that can occur in FEPT when the overlap between production and target method phase spaces is less effective.

The layout of the paper is organized as follows. In the following section, Sec. 2, we

discuss the methodology to couple FEPT and machine learning to obtain quickly and efficiently free energy estimates at multiple levels of theory. In Sec. 3 we introduce the system used to test our new approach (the proton exchange reaction between two oxygen sites in zeolite chabazite) and describe the settings used in numerical simulations. In Sec. 4 we discuss in detail the numerical properties of our method, including performance beyond the expected range of applicability, limitations, and possible improvements. Sec. 5 contains our conclusions.

2 Methodology

In this section we summarize the main theoretical and computational concepts that are at the base of the methodology presented in this paper. Specifically, in Sec. 2.1 we introduce the Helmholtz free energy of activation and show how this quantity can be computed by using the bluemoon sampling method. Starting from MD simulations based on the production method, the value of the activation free energy at the target level of theory can then be obtained by applying free energy perturbation theory (Sec. 2.2). A brute force application of FEPT still requires a significant number of single point calculations using the target approximation. This number can be significantly reduced by training a machine learning algorithm on a small set of explicit calculations and using it to predict all the remaining required values (Sec. 2.3). The canonical (NVT) ensemble is used throughout this study although the generalization of our method for the use with other ensembles is also possible.

2.1 Free energy of activation

The Helmholtz free energy of activation can be expressed using the formula:[3,28]

$$\Delta A^{\ddagger}_{R\to P} = \Delta A_{\xi_{ref,R}\ \to\xi^*} - k_B\,T \ln\left\{\frac{h}{k_B\,T}\frac{\langle|\dot{\xi^*}|\rangle}{2}P(\xi_{ref,R})\right\}, \tag{3}$$

where $\xi = \xi(\boldsymbol{q})$ is the reaction coordinate or its approximation which, in general, depends on all atomic positions $\boldsymbol{q}$, $\xi_{ref,R}$ is the value of ξ for an arbitrary reference point among the reactant configurations, $\dot{\xi}^*$ is the velocity associated with the reaction coordinate for configurations at the transition state (ξ^*), the angular bracket $\langle \cdots \rangle$ represents an ensemble average over all reactant configurations, $P(\xi_{ref,R}) = \langle \delta(\xi_{ref,R} - \xi) \rangle$ is the probability density of $\xi_{ref,R}$ within the ensemble of reactant configurations, and $\Delta A_{\xi_{ref,R} \rightarrow \xi^*} = -k_B T \ln \left\{ \frac{P(\xi^*)}{P(\xi_{ref,R})} \right\}$ is the reversible work needed to shift the reaction coordinate from the value $\xi_{ref,R}$ to ξ^*. We note that Eq. 3 emerges from the combination of the transition state (TS) theory expression for the rate constant[3,29] with the Eyring-Polanyi equation (Eq. 1).

The individual terms of Eq. 3 can be computed by means of molecular dynamics (MD) as follows. The probability density $P(\xi_{ref,R})$ can be approximated by a histogram obtained using the data from a straightforward MD of the reactant state. The term $\Delta A_{\xi_{ref,R} \rightarrow \xi^*}$ can be computed by any simulation method designed to determine free energies of rare events, such as metadynamics,[4] umbrella sampling,[2] or the bluemoon ensemble method.[3] In the present study, we choose the latter method, which seems to be best suited for the purposes of our work (see Sec. 2.2). In this method, free energy differences are determined by integrating free energy gradients along the reaction path connecting the states $\xi_{ref,R}$ and ξ^*:

$$\Delta A_{\xi_{ref,R} \rightarrow \xi^*} = \int_{\xi_{ref,R}}^{\xi^*} \left(\frac{\partial A}{\partial \xi} \right)_{\xi'} d\xi', \tag{4}$$

whereby the free energy gradients are obtained using constrained MD simulations via the following formula:[30]

$$\left(\frac{\partial A}{\partial \xi} \right)_{\xi'} = \frac{1}{\langle Z^{-1/2} \rangle_{\xi'}} \langle Z^{-1/2} [-\lambda + \frac{k_B T}{Z^2} \sum_{i=1}^{N} \sum_{j=1}^{N} \frac{1}{m_i m_j} \sum_{\mu=x,y,z} \sum_{\nu=x,y,z} \frac{\partial \xi}{\partial q_{\mu,i}} \frac{\partial^2 \xi}{\partial q_{\mu,i} \partial q_{\nu,j}} \frac{\partial \xi}{\partial q_{\nu,j}}] \rangle_{\xi'}, \tag{5}$$

where $\langle \cdots \rangle_{\xi'}$ indicates the constrained ensemble average with $\xi(\boldsymbol{q}) = \xi'$, m_i and $q_{\mu,i}$ are the mass and the μ component of a Cartesian position vector of an atom i, respectively, λ is a Lagrange multiplier associated with the parameter ξ used in the SHAKE algorithm,[31] and

Z is the inverse of the mass metric tensor defined as follows:

$$Z = \sum_{i=1}^{N} \frac{1}{m_i} \sum_{\mu=x,y,z} \left(\frac{\partial \xi}{\partial q_{\mu,i}} \right)^2 . \tag{6}$$

The integration of Eq. 4 is performed using the free energy gradients computed for a certain number of points distributed between the states $\xi_{ref,R}$ and ξ^*.

Finally, the generalized velocity term $\langle |\dot{\xi}^*| \rangle$ can be determined using the following equation:[3]

$$\langle |\dot{\xi}^*| \rangle = \sqrt{\frac{2 k_B T}{\pi}} \frac{1}{\langle Z^{-1/2} \rangle_{\xi^*}}, \tag{7}$$

whereby the term $\langle Z^{-1/2} \rangle_{\xi^*}$ is readily available from the constrained MD performed for the state ξ^* within the $\Delta A_{\xi_{ref,R} \rightarrow \xi^*}$ calculation.

2.2 Computing $\Delta A^{\ddagger}$ using free energy perturbation theory

Let us now assume that the free energy of activation $\Delta A^{\ddagger}$ has already been determined as described in Sec. 2.1 using the production method with Hamiltonian $H(\boldsymbol{q}, \boldsymbol{p})$ defined by the potential energy $V(\boldsymbol{q})$ and the kinetic energy $\mathrm{T}(\boldsymbol{p})$. The same quantity determined at the target method level with Hamiltonian $\tilde{H}(\boldsymbol{q}, \boldsymbol{p})$ can be formally expressed as

$$\Delta \tilde{A}^{\ddagger} = \Delta \tilde{A}_{\xi_{ref,R} \rightarrow \xi^*} - k_B T \ln \left(\frac{h}{k_B T} \frac{\langle |\dot{\tilde{\xi}}^*| \rangle}{2} \tilde{P}(\xi_{ref,R}) \right), \tag{8}$$

where a tilde is used to distinguish the quantity computed using the target method from that obtained using the production method. In the following we will suppose that production and target Hamiltonians differ only in position dependent potential energy term, namely $\tilde{H}(\boldsymbol{q}, \boldsymbol{p}) - H(\boldsymbol{q}, \boldsymbol{p}) = \tilde{V}(\boldsymbol{q}) - V(\boldsymbol{q}) = \Delta V(\boldsymbol{q})$. The perturbation $\Delta V(\boldsymbol{q})$ can be introduced not only by changing the physical model that describes the interactions between the particles in the system of interest but also by changing their identity[32] (i.e. via "alchemical transformation"). We show in this section that the target free energy $\Delta \tilde{A}^{\ddagger}$ can be obtained from the

production free energy $\Delta A^{\ddagger}$ in Eq. 3 using FEPT via the following formula:

$$\Delta \tilde{A}^{\ddagger} = \Delta A^{\ddagger} - k_B\,T \ln \left\{ \frac{\langle \exp\left[-\Delta V(\boldsymbol{q})/k_B\,T\right]\rangle_{\xi^*}}{\langle \exp\left[-\Delta V(\boldsymbol{q})/k_B\,T\right]\rangle} \right\}. \tag{9}$$

The expressions $-k_B\,T \ln\left\{\langle \exp\left[-\Delta V(\boldsymbol{q})/k_B\,T\right]\rangle_{\xi^*}\right\}$ and $-k_B\,T \ln\left\{\langle \exp\left[-\Delta V(\boldsymbol{q})/k_B\,T\right]\rangle\right\}$ can be interpreted as corrections to the free energy of TS and R, respectively, and hence we use a shorthand notation ΔA_{TS} and ΔA_R for these two terms throughout this work.

In order to prove Eq. 9, we first express $\Delta \tilde{A}^{\ddagger}$ as $\Delta \tilde{A}^{\ddagger} = \Delta A^{\ddagger} + (\Delta \tilde{A}^{\ddagger} - \Delta A^{\ddagger})$. The term in parenthesis is then obtained by subtracting Eq. 3 from Eq. 8 while making use of the relation $\Delta A_{\xi_{ref,R} \rightarrow \xi^*} = -k_B\,T \ln \frac{P(\xi^*)}{P(\xi_{ref,R})}$ (and analogously for $\Delta \tilde{A}_{\xi_{ref,R} \rightarrow \xi^*}$):

$$\begin{aligned}
\Delta \tilde{A}^{\ddagger} - \Delta A^{\ddagger} &= -k_B\,T \ln \frac{\tilde{P}(\xi^*)}{\tilde{P}(\xi_{ref,R})} + k_B\,T \ln \frac{P(\xi^*)}{P(\xi_{ref,R})} - k_B\,T \ln \frac{\tilde{P}(\xi_{ref,R})}{P(\xi_{ref,R})} - k_B\,T \ln \frac{\langle |\dot{\tilde{\xi}}^*| \rangle}{\langle |\dot{\xi}^*| \rangle} \\
&= -k_B\,T \ln \left\{ \frac{\tilde{P}(\xi^*)}{P(\xi^*)} \times \frac{\langle |\dot{\tilde{\xi}}^*| \rangle}{\langle |\dot{\xi}^*| \rangle} \right\}.
\end{aligned} \tag{10}$$

The ratio between probability densities writes:

$$\begin{aligned}
\frac{\tilde{P}(\xi^*)}{P(\xi^*)} &= \frac{\int d\boldsymbol{p}\, d\boldsymbol{q}\, \delta(\xi(\boldsymbol{q}) - \xi^*) \exp\left[-\Delta V(\boldsymbol{q})/k_B\,T\right] \exp\left[-H(\boldsymbol{p},\boldsymbol{q})/k_B\,T\right]}{\int_{\boldsymbol{q}\in R} d\boldsymbol{p}\, d\boldsymbol{q} \exp\left[-\Delta V(\boldsymbol{q})/k_B\,T\right] \exp\left[-H(\boldsymbol{p},\boldsymbol{q})/k_B\,T\right]} \\
&\times \left(\frac{\int d\boldsymbol{p}\, d\boldsymbol{q}\, \delta(\xi(\boldsymbol{q}) - \xi^*) \exp\left[-H(\boldsymbol{p},\boldsymbol{q})/k_B\,T\right]}{\int_{\boldsymbol{q}\in R} d\boldsymbol{p}\, d\boldsymbol{q} \exp\left[-H(\boldsymbol{p},\boldsymbol{q})/k_B\,T\right]} \right)^{-1},
\end{aligned} \tag{11}$$

where $\boldsymbol{q} \in R$ indicates that the integration is taken over all reactant configurations. Upon a trivial rearrangement, Eq. 11 yields

$$\frac{\tilde{P}(\xi^*)}{P(\xi^*)} = \frac{\langle \delta(\xi(\boldsymbol{q}) - \xi^*) \exp\left[-\Delta V(\boldsymbol{q})/k_B\,T\right]\rangle}{\langle \delta(\xi(\boldsymbol{q}) - \xi^*)\rangle \langle \exp\left[-\Delta V(\boldsymbol{q})/k_B\,T\right]\rangle}. \tag{12}$$

Since we compute the ensemble average $\frac{\langle \delta(\xi(\boldsymbol{q})-\xi^*) \exp[-\Delta V(\boldsymbol{q})/k_B\,T]\rangle}{\langle \delta(\xi(\boldsymbol{q})-\xi^*)\rangle}$

using the constrained molecular dynamics, the following relation[3] must be used to correct

for a bias introduced by fixing the momentum associated with ξ:

$$\frac{\tilde{P}(\xi^*)}{P(\xi^*)} = \frac{\langle Z^{-1/2}\exp\left[-\Delta V(\boldsymbol{q})/k_B\,T\right]\rangle_{\xi^*}}{\langle Z^{-1/2}\rangle_{\xi^*}}\frac{1}{\langle\exp\left[-\Delta V(\boldsymbol{q})/k_B\,T\right]\rangle}. \tag{13}$$

Similarly, the velocity term $\langle|\dot{\xi^*}|\rangle$ computed in a constrained MD with $\xi(\boldsymbol{q}) = \xi^*$ is expressed within the FEPT formalism as follows:

$$\langle|\dot{\tilde{\xi}}^*|\rangle = \sqrt{\frac{2k_B\,T}{\pi}}\frac{\langle\exp\left[-\Delta V(\boldsymbol{q})/k_B\,T\right]\rangle_{\xi^*}}{\langle Z^{-1/2}\exp\left[-\Delta V(\boldsymbol{q})/k_B\,T\right]\rangle_{\xi^*}}. \tag{14}$$

Combining Eq. 14 with Eq. 7, we find the following expression:

$$\frac{\langle|\dot{\tilde{\xi}}^*|\rangle}{\langle|\dot{\xi}^*|\rangle} = \frac{\langle Z^{-1/2}\rangle_{\xi^*}\langle\exp\left[-\Delta V(\boldsymbol{q})/k_B\,T\right]\rangle_{\xi^*}}{\langle Z^{-1/2}\exp\left[-\Delta V(\boldsymbol{q})/k_B\,T\right]\rangle_{\xi^*}}. \tag{15}$$

Finally, Eq. 9 is obtained by plugging Eq. 13 and 15 into Eq. 10.

In general, a direct application of FEPT represents a computationally demanding task as a large number of target method calculations of $\tilde{V}(\boldsymbol{q})$ may be needed in order to obtain well converged reweighted averages in Eq. 9. In this work we propose an efficient solution to this problem based on the MLPT approach introduced in our previous work.[16] The main idea is that most of the time-consuming target method calculations can be avoided by training a Δ-machine learning[33] based model that reliably represents the function $\Delta V(\boldsymbol{q})$. As the number of configurations needed to obtain a good quality $\Delta V(\boldsymbol{q})$ can be, in favorable cases, as small as ten or few tens,[16] the use of the MLPT approach in combination with Eq. 9 represents a highly effective method for computing the free energy barriers (or, more generally, free energy differences) using multiple electronic structure methods.

2.3 Machine learning algorithm

As in our original MLPT method described in Ref. 16, the kernel ridge regression (KRR)[34] machine learning algorithm is used here along with the REMatch kernel[35] defined as

$$K^{\gamma}(A,B) = \mathrm{Tr}\mathbf{P}^{\gamma}\mathbf{C}(A,B), \tag{16}$$

where $\mathbf{P}$ is a doubly stochastic matrix that satisfies the condition

$$\mathbf{P}^{\gamma} = \arg\min_{\mathbf{P}} \sum_{i,j} P_{ij}(1 - C_{ij} + \gamma \ln P_{ij}), \tag{17}$$

and γ is a hyperparameter that controls the entropic contribution. The elements of the covariance matrix $\mathbf{C}(A,B)$ are defined as

$$C_{ij}(A,B) = k(\mathcal{X}_i^A, \mathcal{X}_j^B), \tag{18}$$

where the "local" kernel k provides a measure of the similarity between the $\mathcal{X}_i^A$ and $\mathcal{X}_j^B$ environments belonging to structures A and B, respectively. An environment $\mathcal{X}_i^A$ defined for the structure A of a given material includes the atoms surrounding a specific atom i. In this work, the smooth overlap of atomic positions (SOAP)[35,36] is used to define Eq. 18. Within this approach the density of the atoms (ρ) in the environment $\mathcal{X}_i^A$ is defined as a sum of Gaussians

$$\rho_{\mathcal{X}_i^A}(\mathbf{r}) = \sum_{j \in \mathcal{X}_i^A} \exp\left\{ -\frac{(\mathbf{r} - \mathbf{q}_j)^2}{2\sigma^2} \right\}, \tag{19}$$

with variance σ^2 that are centered at the positions $\mathbf{q}_j$ of all the atoms in the environment $\mathcal{X}_i^A$ with a certain cut-off radius (including the central one). Defining a different environment for each species present in the system, the local SOAP kernel[35,36] is then constructed as an

overlap integral of the densities of pairs of environments

$$\tilde{k}(\mathcal{X}_i^A, \mathcal{X}_j^B) = \int d\hat{R} \left(\int \rho_{\mathcal{X}_i^A}(\mathbf{r}) \rho_{\mathcal{X}_j^B}(\hat{R}\mathbf{r}) d\mathbf{r} \right)^2 . \tag{20}$$

Note that the first integral is performed analytically over the three-dimensional rotations yielding thus a rotationally invariant representation of the system. The normalized kernel

$$k(\mathcal{X}_i^A, \mathcal{X}_j^B) = \frac{\tilde{k}(\mathcal{X}_i^A, \mathcal{X}_j^B)}{\sqrt{\tilde{k}(\mathcal{X}_i^A, \mathcal{X}_i^A)\tilde{k}(\mathcal{X}_j^B, \mathcal{X}_j^B)}} \tag{21}$$

serves as a rotationaly and translationaly invariant measure of similarity whereby the maximum value (one) is attained when the two environments $\mathcal{X}_i^A$ and $\mathcal{X}_j^B$ are identical.

In practice, a certain number of configurations N_{train} is selected to build the REMatch kernel $\mathbf{K}_{train}^{\gamma}$ used to train the ML model:

$$\mathbf{w} = (\mathbf{K}_{train}^{\gamma} + \lambda \mathbf{1})^{-1} \mathbf{y}_{train}, \tag{22}$$

where $\mathbf{y}_{train}$ contains the terms $\Delta V(\boldsymbol{q})$ computed for the configurations in the training set and λ is a regularization hyperparameter used to prevent overfitting. It is important to notice that considering $\Delta V(\boldsymbol{q})$ rather than directly the target method energies is a crucial point to obtain a ML learning algorithm that can be trained with small data sets and whose predictive power extends beyond the expected range of applicability (see Sec. 4.4). Indeed, assuming reasonable statistical correlation between production and target method energies, their difference $\Delta V(\boldsymbol{q})$ presents a rather smooth behavior that allows for a much more efficient learning process. This idea is based on the well established $\Delta-$ML method.[33]

The weights $\mathbf{w}$ obtained from Eq. 22 are used to predict $\Delta V(\boldsymbol{q})$ for all the remaining $\mathrm{N}_{predict} = N_{tot} - N_{train}$ configurations from the MD by applying the following formula:

$$\mathbf{y}_{predict} = \mathbf{K}_{predict}^{\gamma} \mathbf{w}, \tag{23}$$

where $\mathbf{y}_{predict}$ contains the predicted potential energy differences and $\mathbf{K}^{\gamma}_{predict}$ is the $\mathrm{N}_{predict}\times\mathrm{N}_{train}$ REMatch kernel.

3 Computational setting

As a test bench for our new methodology we consider the proton exchange reaction between two oxygen sites in zeolite chabazite. Periodic density-functional calculations for this system have been performed using the VASP code.[37–40] The Kohn-Sham equations have been solved variationally in a plane-wave basis set using the projector-augmented-wave (PAW) method of Blöchl,[41] as adapted by Kresse and Joubert.[42] The calculations have been performed using three different density functional approximation: (i) the PBE exchange-correlation approximation proposed by Perdew et al.[19] is a popular functional from the GGA (generalized gradient approximation) family, (ii) optPBE-vdW[20–23] is an example of a non-local density functional designed to describe long range London dispersion forces, and (iii) HSE06[24–26] is a hybrid functional. These three methods were chosen because they predict distinctly different zero temperature activation energies for the reaction considered here: 0.65 eV (PBE), 0.75 eV (optPBE-vdW), and 0.79 eV (HSE06). Compared to the other two methods, PBE is relatively inexpensive (10-30 times faster when a comparable simulation setting is used) and, accordingly, this functional will be considered as the production method while optPBE-vdW and HSE06 will be used as target methods. In all calculations, a plane wave cutoff of 400 eV was used and the integration in the first Brillouin zone was performed by including the Γ point only. Default PAW potentials were used and projection operators were evaluated in reciprocal space. The convergence criterion for the electronic self-consistency loop was set to 10^{-6} eV/cell.

A primitive rhobohedral cell (space group $R\bar{3}m$) with 37 atoms has been used to represent the zeolite chabazite. The resulting lattice parameters used in calculations ($a = 9.291$ Å and $\alpha = 93.9°$) are close to those reported in previous experimental work[43] on highly silicious

chabazite ($a = 9.304$ Å and $\alpha = 94.6°$). A model with one acid proton and one Al site per a simulation cell has been considered whereby the acid proton was located in position O1, designated according to the nomenclature of Jeanvoine et al.[44]

The integration of Eq. 4 has been performed using the Simpson's method[45] with a mesh of 5 points evenly distributed between the states $\xi_{ref,R}$ and ξ^*. The blue moon ensemble technique as implemented in VASP has been employed.[46] The length of each constrained MD run needed to determine free energy gradient for a given mesh point was 50 ps, whereby the initial period of 20 ps was considered as equilibration and the corresponding data were discarded. In order to avoid possible numerical problems due to the use of a relatively large integration step of 1.0 fs, mass of tritium has been used for all H atoms. The simulation temperature was controlled using the Andersen thermostat[29] with a collision frequency of 0.05 fs^{-1}. The geometric parameter

$$\xi = r_1 - r_2, \tag{24}$$

with r_1 and r_2 being defined in Fig. 1, was used as an approximation to the reaction coordinate of our model reaction. The length of unconstrained MD simulations of reactant was 100 ps, whereby the same simulation setting as in constrained runs was used.

The numerical implementation of the ML models considered in this work is based on the DScribe libraries.[47,48] Drawings of structures presented in this work have been created using the program VESTA.[49]

4 Results and discussion

4.1 Production and reference calculations

Fig. 2 (left panel) shows the free energy profile ($\Delta A(\xi)$) computed using the PBE functional (the production method) for temperature T=600 K. As a reference state, the point $\xi_{ref,R} =$

-1.546 Å has been chosen corresponding to a high probability density state (see Fig. 2 (right panel)). We emphasize that the choice of the reference state $\xi_{ref,R}$ can not affect the value of computed $\Delta A^{\ddagger}$ (see Appendix A) and hence we are free to choose any arbitrary reactant state for this purpose. The symmetry of the problem (see Fig. 1) largely determines the geometry of the free energy transition state, fixing the value of ξ^* at $\sim$0 Å, and the choice of the electronic structure method turns out to have only a negligible effect on this value. Hence instead of refining the value of ξ^* for each method, we simply used the value of -0.026 Å found by the zero T relaxation of transition state at the PBE level. We show in Sec. SI in Supporting Information that the error introduced by fixing ξ^* is negligible. The free energy of activation computed using the production method at 600 K is 0.66 eV.

In order to define an "exact" reference (Reference A) for our further analysis, we performed full MD simulations also for the two target methods (i.e. optPBE-vdW and HSE06 in this work). While the aim of our methodology is to avoid MD simulations based on expensive target methods, in this paper Reference A will help to establish the accuracy of perturbation theory. As shown in Tab. 1, the free energies of activation increase by 0.09 eV and 0.14 eV when the PBE method is replaced by optPBE-vdW and HSE06, respectively.

In order to distinguish the error introduced by ML from that of FEPT itself, we also introduce another reference (Reference B) created by a brute force application (i.e. performing explicit target method calculations instead of predicting the results with the ML model) of the FEPT procedure to a large number of data points from the production run. To this end, we defined a set (hereafter designated as a test set) consisting of every tenth configuration from the production MD run. For each of the 5000 (TS) or 10000 (R) points of the test set, a target method calculation was performed and the potential energy difference $\Delta V(\boldsymbol{q})$ was computed. In order to apply Eq. 9, two independent test sets have been defined: one for the transition ($\xi = \xi^*$) and another one for the unconstrained reactant state. In principle, the difference in the results of Referece A and B reflects the systematic error introduced by a possibly ineffective application of perturbation theory.[32] In the case of the optPBE-vdW

target method, the Reference A and B results agree within 0.003 eV showing that the simple forward FEPT scheme used in this study is sufficient. A slightly more significant difference (0.028 eV) is found for the HSE06 method suggesting that the overlap between configurations generated by the production and target methods might be suboptimal (see Sec. SII in the Supporting Information). As we discuss in Sec. 4.5, this problem can be reduced by using more sophisticated sampling methods,[50] which can greatly benefit from the ML acceleration.

For the needs of presentation in Sec. 4.3, production, Reference A, and Reference B calculations have been performed also for T=300 K. The corresponding numerical values are compiled in Tab. 3 and the free energy profiles and probability distributions used in $\Delta A^{\ddagger}_{R\to P}$ calculations are presented in Sec. SIII of Supporting Information.

4.2 Performance of the MLPT method in free energy perturbation theory calculations

As also discussed in Sec. 4.5, a direct application of FEPT could require a large number of target method calculations. Here we show how most of these explicit calculations can be effectively and inexpensively replaced by the predictions of a MLPT model. As a first step of this approach, a certain number (N_{train}) of configurations is selected out of the MD data generated with the production method. For these configurations single point calculations using target methods are performed and the corresponding results are used to train the ML algorithm described in Sec. 2.3. In principle, the free energy results obtained via this procedure should ultimately converge to those of Reference B (see Sec. 4.1) as the accuracy of the predictions improves by increasing the size of the training set. In this section we examine the performance of the MLPT method and compare it with that of the straightforward FEPT (namely without ML). We focus here on the ΔA_{TS} term (see Sec. 2.2) for the transition state computed at the HSE06 level of theory but similar conclusions can be drawn also for the reactant term ΔA_R as well as for the other target method optPBE-vdW (see Sec. SIV in the Supporting Information). For our study we considered different sizes

of the training set with $N_{train} = 10, 20, 50$, and 100. Although a carefully chosen selection strategy can lead to significantly improved performance in some applications,[6] the choice of the specific training configurations contained in a set is to some extent arbitrary. To understand the importance of this choice, for each value of N_{train} we considered 100 different realizations of the training set. Specifically, to generate the different sets we selected at random N_{train} configurations (separated from each other by at least 100 MD steps) and repeated this procedure 100 times. The ΔA_{TS} free energies for all sets of size N_{train} were then computed both by direct application of FEPT (namely only on N_{train} configurations without ML predictions) or by using the MLPT approach. For each value of N_{train} the values obtained from the different sets were then averaged and standard deviation was used as a measure of dispersion of individual results. These data, which are presented in Tab. 2, indicate that the straightforward FEPT tend to converge to a correct average result, which is close to the Reference B (see Sec. 4.1), with increasing number of configurations used in the calculation. Nevertheless, the convergence is slow and the individual results for each of the 100 sets are spread over broad intervals of widths ranging between ∼0.50 eV for N_{train}=10 and ∼0.15 eV for N_{train}=100 (these numbers are well over the chemical accuracy threshold of 1 kcal/mol=0.043 eV). This behavior, which is also clearly illustrated in Fig. 3 for N_{train}=50, leads to the large standard deviations of the FEPT results in Tab. 2. Clearly, such a large uncertainty in predicted results (even larger than the difference in actual free energies of activation between the methods considered here) makes the straightforward application of the FEPT method unreliable when only small sets of data can be used.

On the other side it is evident from the data presented in Tab. 2 that the use of machine learning reduces the uncertainty in ΔA_{TS} significantly, leading to a dramatic reduction in the standard deviations (at least by a factor of two) as compared to the straightforward FEPT. Just like in the case of straightforward FEPT calculations, however, the averaged free energies are systematically shifted to higher values. This trend of MLPT to overestimate ΔA_{TS} is also evident in Fig. 3 for the results obtained using the different N_{train}=50 sets.

Although this systematic error decreases by increasing the accuracy of the ML predictions (becoming basically negligible for N_{train}=100), it is highly desirable to develop a correction scheme to reduce this behavior. To better understand the origin of this systematic deviation and correct it, let us substitute the term $\Delta V(\boldsymbol{q})$ in the second order cumulant approximation of free energy:[51]

$$\tilde{A} - A \approx \langle \Delta V(\boldsymbol{q}) \rangle - \frac{\langle \Delta V^2(\boldsymbol{q}) \rangle - \langle \Delta V(\boldsymbol{q}) \rangle^2}{k_B\, T} \tag{25}$$

by $\Delta V'(\boldsymbol{q}) + \epsilon(\boldsymbol{q})$, where $\Delta V'(\boldsymbol{q})$ is the potential energy difference predicted by ML and $\epsilon(\boldsymbol{q})$ is the error in the prediction made by ML for the configuration $\boldsymbol{q}$. Upon a trivial algebraic manipulation, we arrive at the following expression:

$$\Delta A_{TS} = \Delta A'_{TS} + \Delta_\epsilon, \tag{26}$$

where

$$\Delta A'_{TS} \;=\; \langle \Delta V'(\boldsymbol{q}) \rangle_{\xi^*} - \frac{\langle (\Delta V'(\boldsymbol{q}))^2 \rangle_{\xi^*} - \langle \Delta V'(\boldsymbol{q}) \rangle^2_{\xi^*}}{2\, k_B\, T} \tag{27}$$

represents the (biased) MLPT prediction obtained by using $\Delta V'(\boldsymbol{q})$ and

$$\Delta_\epsilon \;=\; \langle \epsilon \rangle_{\xi^*} - \frac{\langle \epsilon \rangle_{\xi^*} - \langle \epsilon \rangle^2_{\xi^*}}{2\, k_B\, T} - \frac{\langle \epsilon\, (\Delta V'(\boldsymbol{q})) \rangle_{\xi^*} - \langle \epsilon \rangle_{\xi^*} \langle \Delta V'(\boldsymbol{q}) \rangle_{\xi^*}}{k_B\, T}, \tag{28}$$

is a systematic error due to the random error associated with the ML predictions. Following the idea developed by Rocca et al.,[16] we estimate the error Δ_ϵ for our MLPT calculations by using a fixed correction set of N_{corr}=10 points not included in the training set (i.e., all integrals $\langle \cdots \rangle$ are approximated by $\left(1/N_{corr} \sum_i^{N_{corr}} \cdots \right)$ where the summation runs over all members of the correction set). As shown in Tab. 2 and Fig. 3, our simple correction procedure essentially eliminates the systematic error in calculations performed with the small training sets. Importantly, the statistical uncertainty of the MLPT remains small in comparison to the straingthforward FEPT, as obvious from small values of standard deviation

presented in Tab. 2. Altogether, our numerical tests showed that the MLPT approach can yield accurate results already for small training sets and, importantly, the corresponding statistical uncertainty given by a particular choice of the training set is significantly reduced compared to the straightforward FEPT. An interesting implication of the form of correction (Eq. 28) is that the error introduced to $\Delta\tilde{A}^{\ddagger}$ due to inaccurate ML model for TS tends to cancel that from the model for R if the quality of both models is similar. Indeed, the convergence of $\Delta\tilde{A}^{\ddagger}$ with the size of training set is often faster than that of ΔA_{TS} or ΔA_R.

Having explored the properties of the MLPT scheme, we can now proceed to the determination of the free energy of activation for T=600 K. To this end, the training set N_{train}=100 is used, which yields reliable predictions for both ΔA_R and ΔA_{TS} (see Sec. SIV in the Supporting Information). As obvious from the data summarized in Tab. 1, the free energies of activation computed for both target methods are in excellent agreement with the corresponding Reference B values. A somewhat larger difference with respect to the exact result (Reference A) in the case of the HSE06 method can be reduced by using a more sophisticated algorithm for the realization of perturbation theory calculations. We will return to this point in Sec. 4.5.

4.3 Changing the simulation temperature

The configuration space sampled at a lower temperature represents often a subset of that sampled at a higher T. This is illustrated by Fig. 4, where the probability distributions computed for the distances r_1 and r_2 (cf. Fig. 1) at T=300 K and T=600 K are compared. It is reasonable to expect that a ML model trained to reliably describe the property of interest for a broader set of configurations should work well also for its subsets. This property can be exploited within the MLPT method to obtain free energies in a wide range of temperatures with a significant reduction of computational time by avoiding additional target method calculations. Once the MLPT approach has been applied to a broader high-temperature set, free energies at lower temperatures can be obtained by performing only cheap produc-

tion method MDs and using the same ML model to predict the $\Delta V(\boldsymbol{q})$'s without further retraining. As an illustrative example of such a procedure, we shall consider a calculation of the free energy of activation of our reference reaction at the temperature of T=300 K. To this end, we employ the ML model trained for the configurations generated at 600 K (see Sec. 4.2) and the only additional calculations that we perform are the production method MD simulations at 300 K. In Sec. SV of Supporting Information we show that the use of the ML model trained at a higher T leads to only modest deterioration of the quality of the $\Delta V(\boldsymbol{q})$ predictions for lower temperature. As shown in Tab. 3, the computed MLPT results are in a good agreement with the corresponding Reference B (see Sec. 4.1), indicating that our MLPT scheme is indeed successful in avoiding additional target method calculations needed to achieve converged free energies at lower temperature.

4.4 Extending the machine learning predictions beyond the training set scope

In this section we explore the possibility to use the models trained specifically for the ΔA_{TS} and ΔA_R calculations to estimate the differences (both terms on the left hand side are defined analogously to Eq. 4):

$$\begin{aligned} \Delta\tilde{A}_{\xi_{ref,R}\rightarrow\xi'} - \Delta A_{\xi_{ref,R}\rightarrow\xi'} &= -k_B T \ln \frac{\langle Z^{-1/2} \exp\left[-\Delta V(\boldsymbol{q})/k_B T\right]\rangle_{\xi'}}{\langle Z^{-1/2}\rangle_{\xi'}} \\ &+ k_B T \ln \frac{\langle Z^{-1/2} \exp\left[-\Delta V(\boldsymbol{q})/k_B T\right]\rangle_{\xi_{ref,R}}}{\langle Z^{-1/2}\rangle_{\xi_{ref,R}}}, \end{aligned} \tag{29}$$

for arbitrary intermediate states $\xi = \xi'$. Such a correction is useful when full free energy profiles such as those shown in Fig. 2 are needed, in which case the last constant term on the right hand side of Eq. 29 becomes irrelevant (as the profile can always be shifted by an arbitrary constant). In particular, by using MLPT we shall attempt here to estimate the full free energy profile for the target method HSE06 using only the data presented in Sec. 4.1, i.e., without performing any additional target calculations. To this end, we examine three

different strategies for the training set selection restricted here to the size of N_{train} =100 configurations.

In our first test, we employ a ML model trained using 100 transition state configurations to predict free energies of all 4 remaining points considered in our bluemoon ensemble simulations. As the training set configurations are very different from the other intermediate states, this strategy is expected to fail and we consider it here only for illustrative purposes. Fig. 5 and the statistical data presented in Tab. S10 show that the free energy profile predicted in this way is indeed very inaccurate and the quality of the predictions decreases with the distance of given microstate from the TS. The largest root mean square error (RMSE) in $\Delta V(\boldsymbol{q})$ computed with respect to the Reference B is as large as 0.108 eV.

Somewhat surprisingly then, the performance of the model trained on 100 reactant configurations performs relatively well and the predicted free energy profile is close to that obtained from Reference B (see Fig. 5). As before, the quality of predictions decreases with the distance from the state for which the ML was trained and the largest value of the RMSE (0.039 eV) is found for the states close to TS.

Finally, the best performance is found for the training set composed of 50 reactant and 50 transition state configurations. With this training set, a consistent quality of $\Delta V(\boldsymbol{q})$ predictions is achieved for all intermediate states with the largest RMSE being reduced by about a factor two compared to the predictions made with ML trained on reactant configurations (see Tab. S10 of Supporting Information).

The ability of the ML scheme to make reliable predictions also for the parts of configuration space beyond those spanned by the training set demonstrated in this section can be used in many different ways, e.g., for refining of TS position, which may vary with the choice of the target method. An example of another application making use of this property is presented in Sec. 4.5, where we propose a scheme to improve accuracy of our FEPT predictions.

4.5 Improving the accuracy of free energy perturbation theory calculations

While formally exact, FEPT is in practice based on MD simulations that span a finite time interval and, accordingly, a limited part of configurational space. This is at the origin of errors that manifest themselves as deviations between Reference B and Reference A (see Sec. 4.1). Although MLPT allows for a fast convergence towards the Reference B free energies with only few tens of target method calculations, its straightforward application cannot overcome the intrinsic limitations of FEPT. As discussed in detail in Sec. SII in Supporting Information, a worse performance of FEPT in calculations with the HSE06 target method as compared to optPBE-vdW is caused by the fact that the phase space overlap with the production method is much smaller. This in turn means that the configurations receiving the highest reweighting factors $\exp\left[-\Delta V(\boldsymbol{q})/k_B\,T\right]$, contributing thus most significantly to the resulting target method free energy, are generated only rarely by the production method, leading thus to a slow convergence with respect to the number of configurations. An effective solution to this problem is to use a multistage sampling[52] where one or more intermediate states are introduced so as to improve the overlaps between the phase space distributions of intermediate states and the distributions generated by the production and target methods. One of the simplest realizations of this idea is represented by the Simple Overlap Sampling (SOS) method[53] where a single intermediate state M is chosen such that the corresponding Hamiltonian fulfills the condition $H_M = (H + \tilde{H})/2$. The corresponding expression for the difference in free energies of activation (cf. Eq. 9) between the production and target methods then writes:

$$\begin{aligned}\Delta\tilde{A}^{\ddagger} - \Delta A^{\ddagger} &= -k_B\,T \ln\left\{\frac{\langle\exp\left[-\Delta V(\boldsymbol{q})/2k_B\,T\right]\rangle_{\xi^*,H}}{\langle\exp\left[-\Delta V(\boldsymbol{q})/2k_B\,T\right]\rangle_{H}}\right\} \\ &+ k_B\,T \ln\left\{\frac{\langle\exp\left[\Delta V(\boldsymbol{q})/2k_B\,T\right]\rangle_{\xi^*,\tilde{H}}}{\langle\exp\left[\Delta V(\boldsymbol{q})/2k_B\,T\right]\rangle_{\tilde{H}}}\right\},\end{aligned} \tag{30}$$

where $\langle \cdots \rangle_H$ and $\langle \cdots \rangle_{\tilde{H}}$ indicate canonical ensemble averages corresponding to Hamiltonians H and $\tilde{H}$, respectively. In order to establish the effect of the SOS correction we have generated reference results (denoted as Reference B (SOS)) obtained by a brute-force evaluation of Eq. 30. As shown in Tab. 1, the application of the SOS decreases the deviation of the bare Reference B value with respect to the "exact" Reference A from 0.028 eV to 0.004 eV.

For the specific goals of the present work, a direct use of Eq. 30 as done to obtain Reference B (SOS) turns out to be disadvantageous as it requires the sampling to be performed at both the production (H Hamiltonian) and target ($\tilde{H}$) method levels. However, one can design a simulation protocol in which the potentially CPU heavy target method sampling is performed with the aid of the MLPT method at the cost of the production method calculation. In this respect, the ability of the MLPT method to reliably predict energies of configurations outside the configuration space spanned by the training set, demonstrated in Sec. 4.4, turns out to be very useful. Specifically, it is crucial for our purposes that the ML model trained on R or TS configurations generated by the production method canonical ensemble sampling allows for reasonable $\Delta V(\boldsymbol{q})$ predictions also for the configurations that would be generated by the target method sampling.

Our tests done on the ML model trained using 100 HSE06 energies corresponding to R or TS configurations generated by the production method show that this is indeed the case. For R the RMSE in the predictions of this model is 0.018 eV for PBE-generated configurations and 0.015 eV for HSE06 configurations; analogously, for TS we have 0.019 eV and 0.018 eV, respectively. Furthermore, Fig. 6 shows that the ML model trained using the configurations generated by the production method generates correct $\Delta V(\boldsymbol{q})$ distributions also for the configurations generated by the target method.

Based on the observations described above, we devise a simulation protocol in which we determine the computationally demanding terms $\langle \exp\left[-\frac{\Delta V(\boldsymbol{q})}{2k_B T}\right] \rangle_{\tilde{H}}$ needed in Eq. 30 by means of the Metropolis Monte Carlo (MC) algorithm.[29] Within this approach the target method

potential energy $\tilde{V}(\boldsymbol{q}) = V(\boldsymbol{q}) + \Delta V(\boldsymbol{q})$ of each configuration is obtained by predicting $\Delta V(\boldsymbol{q})$ using the same ML model for reactant or transition state configurations discussed in Secs. 4.2 and 4.3. Randomly generated Maxwell-Boltzmann distributed velocities multiplied by a time step (Δt=1 fs) chosen so as to achieve the acceptance rate of ∼50 % were used to produce atomic displacements needed in the MC procedure. In the case of constrained TS simulation, the value of $\xi(\boldsymbol{q}) = \xi^*$ was fixed by using the SHAKE algorithm.[31] Altogether, 100000 MC steps have been performed out of which the initial 20000 steps were considered as equilibration. As shown in Tab. 1, the free energies of activation predicted by MLPT at 600 K combined with the SOS scheme are in excellent agreement with the Reference B (SOS) data. We further stress here that these MLPT results were obtained from previously trained ML models without any additional target method calculations. The ML-based strategy described here can be easily adapted for the use with more sophisticated schemes combining the forward and backward sampling, such as the Bennett acceptance ratio method,[54] or with the multistage stratification schemes.[50] Finally we note that, in principle, a similar strategy could be used to improve the MLPT results for the HSE06 target method at 300 K. However, due to a very poor phase space overlap between the distributions generated by the production and target methods (see Sec. SII in the Supporting Information), a multistage sampling with more than one intermediate would be needed.

5 Conclusions

We proposed a new method that couples machine learning and perturbation theory to efficiently compute free energies at multiple levels of theory and possibly also employing quantum chemical approaches that would normally be considered too expensive. Starting from a numerically affordable production method, free energies at different levels of theory can be obtained by performing only a few tens of single point energy calculations, which is achieved by complementing the small number of results with the predictions of a machine learning

model. Remarkably, the extra calculations need to be performed only for the initial (reactant) and the final (transition state) states of the process of interest. The great potential of this method is demonstrated by computing the free energy of activation for the proton exchange reaction in chabazite. The ML model that we developed provides accurate predictions also beyond the range of applicability that could be expected from the training set. This observation has been exploited to inexpensively evaluate free energies at different temperatures and to devise a correction scheme when FEPT does not reach a fully satisfactory level of accuracy.

In this work we primarily focused on the free energies of activation but the generalization of our method to free energy differences between two stable states ($\Delta\tilde{A}_{R\to P}$) is straightforward. By the similar arguments as used in Sec. 2.2, it is easy to prove the following equality

$$\Delta\tilde{A}_{R\to P} = \Delta A_{R\to P} - k_B\,T \ln\left\{\frac{\langle \exp\left[-\Delta V(\boldsymbol{q})/k_B\,T\right]\rangle_P}{\langle \exp\left[-\Delta V(\boldsymbol{q})/k_B\,T\right]\rangle_R}\right\}, \tag{31}$$

where $\langle\cdots\rangle_R$ and $\langle\cdots\rangle_P$ indicate ensemble averages over initial and final stable states, respectively.

Finally, the schemes to access the free energy of chemical reactions by multiple levels of theory have been proposed in several previous publications and we wish to comment here on the relation of our method to these previously published works. The common feature of our method with those of Shen et al.,[10] Li et al.,[11] and Piccini and Parrinello[13] is the use of FEPT to determine the free energy at the level of theory different from that at which the sampling of configuration space has been performed. Another feature common with some previous reports is the use of the machine learning in the calculation. Similar to our work, Shen et al.[10] employed ML to compute $\Delta V(\boldsymbol{q})$ needed in the FEPT calculations. An alternative usage of ML reported in the context free energy calculations of chemical reactions involves acceleration of the configuration space sampling[12] and effective smoothing of free energy profiles at the post-processing stage.[11] The problem of ineffective phase space overlap between the production and target methods (which we discus in Sec. 4.5) has been

addressed by Shen and Yang[12] and Pan et al.[14] Despite sharing some common features, our method differs in several important details from the schemes proposed previously. Most importantly, our method is primarily designed to determine free energy of activation (Eq. 3) rather than the free energy profile (Eq. 29) considered in the previous work.[10–14] Although the two quantities are related, because the knowledge of $\Delta A_{\xi_{ref,R} \rightarrow \xi'}$ allows for calculation of $\Delta A_{\xi_{ref,R} \rightarrow \xi^*}$ needed in Eq. 3, the expression for $\Delta A^{\ddagger}_{R \rightarrow P}$ contains also additional terms $\langle |\dot{\xi^*}| \rangle$ and $P(\xi_{ref,R})$ whose calculation has not been discussed in Refs.[10–14] In our work, we show for the first time that FEPT can be efficiently combined with ML to compute $\Delta A^{\ddagger}_{R \rightarrow P}$ when bluemoon ensemble technique is used, leading to disarmingly simple expression Eq. 9 containing only the perturbation terms for the free reactant and constrained transition state. Since only the energetics of reactant and TS (but not that of any intermediate state) is relevant according to this formula, two independent ML models can be used for these two states to accelerate the FEPT calculations employing only a very small number of training configurations. This is a very important difference compared to other methods where FEPT (with or without ML acceleration) was employed to study activated processes,[10,11,13] in which the target method calculations were performed also for many intermediate states. We note that the fact that training of ML is necessary only for the two thermodynamic states located at the end points of the transformation path, but not for the intermediate points, was realized also by Jinnouchi et al.[8] in a the context of calculations of chemical potential of Si and LiF in water via thermodynamic integration.

Another original contribution presented in our work is the analysis of effect of systematic error introduced by the ML model on the free energy computed perturbatively. We derived a simple correction (Eq. 28) that allows for an inexpensive reduction of this error. In connection with our target quantity $\Delta A^{\ddagger}_{R \rightarrow P}$, it is important to note that the form of Eq. 28 suggests that the error introduced by the inaccurate ML model for TS cancels with that for R if the quality of models trained for both states is similar. This result provides explanation for our empirically observed fact that the convergence of $\Delta A^{\ddagger}_{R \rightarrow P}$ with respect to the training set

size is faster than that of the individual free energy correction terms for TS and R.

Altogether, the ML-based approach proposed in this work is general and holds the promise to improve the accuracy of ab initio free energy calculations for many applications in chemistry and materials science.

6 Acknowledgements

T.B. acknowledges support from Slovak Research and Development Agency under the Contracts No. APVV-15-0105 and No. VEGA-1/0777/19. D.R. acknowledges financial support through the COMETE project (COnception in silico de Matériaux pour l'EnvironnemenT et l'Energie) co-funded by the European Union under the program "FEDER-FSE Lorraine et Massif des Vosges 2014-2020". Part of the results of this research have been achieved using the Computing Center of the Slovak Academy of Sciences acquired in projects ITMS 26230120002 and 26210120002 supported by the Research and Development Operational Program funded by the ERDF.

Supporting Information Available

The Supporting Information is available free of charge on the ACS Publications website at [URL will be inserted by ACS]. Validity of frozen TS approximation, analysis of accuracy of FEPT calculations, reference A calculations for T=300 K, analysis of performance of the MLPT method at 600 K, performance of MLPT models at 300 K, accuracy of MLPT extended beyond the training set scope.

A Independence of $\Delta A^{\ddagger}_{R\to P}$ on the choice of the reference state

Let us consider two different choices of reference states labeled as $\xi_{ref,R}$ and $\xi_{ref,R'}$ and let us rewrite Eq. 3 as follows:

$$\begin{aligned}\Delta A^{\ddagger} &= \Delta A_{\xi_{ref,R'}\to\xi^*} - k_B\,T\ln\left(\frac{h}{k_B\,T}\frac{\langle|\dot{\xi^*}|\rangle}{2}P(\xi_{ref,R'})\right)\\ &+ \Delta A_{\xi_{ref,R}\to\xi_{ref,R'}} + k_B\,T\ln\left(\frac{P(\xi_{ref,R'})}{P(\xi_{ref,R})}\right).\end{aligned}$$

The last two terms on the right hand side cancel each other because, by definition,

$$\Delta A_{\xi_{ref,R}\to\xi_{ref,R'}} = -k_B\,T\ln\left(\frac{P(\xi_{ref,R'})}{P(\xi_{ref,R})}\right)$$

leading to a desired result

$$\begin{aligned}\Delta A^{\ddagger} &= \Delta A_{\xi_{ref,R}\to\xi^*} - k_B\,T\ln\left(\frac{h}{k_B\,T}\frac{\langle|\dot{\xi^*}|\rangle}{2}P(\xi_{ref,R})\right)\\ &= \Delta A_{\xi_{ref,R'}\to\xi^*} - k_B\,T\ln\left(\frac{h}{k_B\,T}\frac{\langle|\dot{\xi^*}|\rangle}{2}P(\xi_{ref,R'})\right)\end{aligned}$$

proving the independence of $\Delta A^{\ddagger}$ on the choice of the reference reactant state.

References

(1) Atkins, P.; de Paula, J. *Atkins' physical chemistry*; Oxford university press: San Diego, 2002; pp 956–963.

(2) Torrie, G.; Valleau, J. Nonphysical sampling distributions in Monte Carlo free-energy estimation: Umbrella sampling. *J. Comput. Phys.* **1977**, *23*, 187 – 199.

(3) Carter, E.; Ciccotti, G.; Hynes, J.; Kapral, R. Constrained reaction coordinate dynamics for the simulation of rare events. *Chem. Phys. Lett.* **1989**, *156*, 472–477.

(4) Laio, A.; Parrinello, M. Escaping free-energy minima. *Proc. Natl. Acad. Sci. U.S.A.* **2002**, *99*, 12562–12566.

(5) Bartlett, R. J.; Musial, M. Coupled-cluster theory in quantum chemistry. *Rev. Mod. Phys.* **2007**, *79*, 291–352.

(6) Bartók, A. P.; De, S.; Poelking, C.; Bernstein, N.; Kermode, J. R.; Csányi, G.; Ceriotti, M. Machine learning unifies the modeling of materials and molecules. *Sci. Adv.* **2017**, *3*, e1701816.

(7) Cheng, B.; Engel, E. A.; Behler, J.; Dellago, C.; Ceriotti, M. Ab initio thermodynamics of liquid and solid water. *Proc. Natl. Acad. Sci.* **2019**, *116*, 1110–1115.

(8) Jinnouchi, R.; Karsai, F.; Kresse, G. Making free-energy calculations routine: Combining first principles with machine learning. *Phys. Rev. B* **2020**, *101*, 060201.

(9) Gao, J. Absolute free energy of solvation from Monte Carlo simulations using combined quantum and molecular mechanical potentials. *J. Phys. Chem.* **1992**, *96*, 537–540.

(10) Shen, L.; Wu, J.; Yang, W. Multiscale Quantum Mechanics/Molecular Mechanics Simulations with Neural Networks. *J. Chem. Theory Comput.* **2016**, *12*, 4934–4946.

(11) Li, P.; Jia, X.; Pan, X.; Shao, Y.; Mei, Y. Accelerated Computation of Free Energy Profile at ab Initio Quantum Mechanical/Molecular Mechanics Accuracy via a Semi-Empirical Reference Potential. I. Weighted Thermodynamics Perturbation. *J. Chem. Theory Comput.* **2018**, *14*, 5583–5596.

(12) Shen, L.; Yang, W. Molecular Dynamics Simulations with Quantum Mechanics/Molecular Mechanics and Adaptive Neural Networks. *J. Chem. Theory Comput.* **2018**, *14*, 1442–1455.

(13) Piccini, G.; Parrinello, M. Accurate Quantum Chemical Free Energies at Affordable Cost. *J. Phys. Chem. Lett.* **2019**, *10*, 3727–3731.

(14) Pan, X.; Li, P.; Ho, J.; Pu, J.; Mei, Y.; Shao, Y. Accelerated computation of free energy profile at ab initio quantum mechanical/molecular mechanical accuracy via a semi-empirical reference potential. II. Recalibrating semi-empirical parameters with force matching. *Phys. Chem. Chem. Phys.* **2019**, *21*, 20595–20605.

(15) Zwanzig, R. W. High-Temperature Equation of State by a Perturbation Method. I. Nonpolar Gases. *J. Chem. Phys.* **1954**, *22*, 1420–1426.

(16) Chehaibou, B.; Badawi, M.; Bučko, T.; Bazhirov, T.; Rocca, D. Computing RPA Adsorption Enthalpies by Machine Learning Thermodynamic Perturbation Theory. *J. Chem. Theory Comput.* **2019**, *15*, 6333–6342.

(17) Fermann, J. T.; Auerbach, S. Modeling proton mobility in acidic zeolite clusters: II. Room temperature tunneling effects from semiclassical rate theory. *J. Chem. Phys.* **2000**, *112*, 6787–6794.

(18) Sierka, M.; Sauer, J. Proton mobility in Chabazite, Faujasite, and ZSM-5 Zeolite catalysts. Comparison based on ab initio calculations. *J. Phys. Chem. B* **2001**, *105*, 1603–1613.

(19) Perdew, J. P.; Burke, K.; Ernzerhof, M. Generalized gradient approximation made simple. *Phys. Rev. Lett.* **1996**, *77*, 3865–3868.

(20) Dion, M.; Rydberg, H.; Schröder, E.; Langreth, D. C.; Lundqvist, B. I. Van der Waals Density Functional for General Geometries. *Phys. Rev. Lett.* **2004**, *92*, 246401.

(21) Román-Pérez, G.; Soler, J. M. Efficient Implementation of a van der Waals Density Functional: Application to Double-Wall Carbon Nanotubes. *Phys. Rev. Lett.* **2009**, *103*, 096102.

(22) Klimeš, J.; Bowler, D. R.; Michaelides, A. Chemical accuracy for the van der Waals density functional. *J. Phys. Condens. Matter* **2009**, *22*, 022201.

(23) Klimeš, J.; Bowler, D. R.; Michaelides, A. Van der Waals density functionals applied to solids. *Phys. Rev. B* **2011**, *83*, 195131.

(24) Heyd, J.; Scuseria, G. E.; Ernzerhof, M. Hybrid functionals based on a screened Coulomb potential. *J. Chem. Phys.* **2003**, *118*, 8207–8215.

(25) Heyd, J.; Scuseria, G. E.; Ernzerhof, M. Erratum: "Hybrid functionals based on a screened Coulomb potential" [J. Chem. Phys. 118, 8207 (2003)]. *J. Chem. Phys.* **2006**, *124*, 219906.

(26) Paier, J.; Hirschl, R.; Marsman, M.; Kresse, G. The Perdew–Burke–Ernzerhof exchange-correlation functional applied to the G2-1 test set using a plane-wave basis set. *J. Chem. Phys.* **2005**, *122*, 234102.

(27) Mangiatordi, G. F.; Brémond, E.; Adamo, C. DFT and Proton Transfer Reactions: A Benchmark Study on Structure and Kinetics. *J. Chem. Theory Comput.* **2012**, *8*, 3082–3088.

(28) Bucko, T.; Chibani, S.; Paul, J.-F.; Cantrel, L.; Badawi, M. Dissociative iodomethane

adsorption on Ag-MOR and the formation of AgI clusters: an ab initio molecular dynamics study. *Phys. Chem. Chem. Phys.* **2017**, *19*, 27530–27543.

(29) Frenkel, D.; Smit, B. *Understanding molecular simulation: from algorithms to applications*; Academic press: San Diego, 2002; pp 436–450.

(30) Sprik, M.; Ciccotti, G. Free energy from constrained molecular dynamics. *J. Chem. Phys.* **1998**, *109*, 7737–7744.

(31) Ryckaert, J.; Ciccotti, G.; Berendsen, H. Numerical-integration of Cartesian equations of motion of a system with constraints - molecular-dynamics of n-alkanes. *J. Comp. Phys.* **1977**, *23*, 327–341.

(32) Lu, N.; Woolf, T. B. In *Free energy calculations: Theory and Applications in Chemistry and Biology*; Chipot, C., Pohorille, A., Eds.; Springer-Verlag Berlin Heidelberg, 2007; pp 203–215.

(33) Ramakrishnan, R.; Dral, P. O.; Rupp, M.; von Lilienfeld, O. A. Big data meets quantum chemistry approximations: The Δ-machine learning approach. *J. Chem. Theory Comput.* **2015**, *11*, 2087–2096.

(34) Rupp, M. Machine learning for quantum mechanics in a nutshell. *Int. J. Quantum Chem.* **2015**, *115*, 1058–1073.

(35) De, S.; Bartók, A. P.; Csányi, G.; Ceriotti, M. Comparing molecules and solids across structural and alchemical space. *Phys. Chem. Chem. Phys.* **2016**, *18*, 13754–13769.

(36) Bartók, A. P.; Kondor, R.; Csányi, G. On representing chemical environments. *Phys. Rev. B* **2013**, *87*, 184115.

(37) Kresse, G.; Hafner, J. Ab-initio molecular-dynamics for open-shell transition-metals. *Phys. Rev. B* **1993**, *48*, 13115–13118.

(38) Kresse, G.; Hafner, J. Ab-initio molecular-dynamics simulation of the liquid-metal amorphous-semiconductor transition in germanium. *Phys. Rev. B* **1994**, *49*, 14251–14269.

(39) Kresse, G.; Furthmüller, J. Efficiency of ab-initio total energy calculations for metals and semiconductors using a plane-wave basis set. *Computat. Mater. Sci.* **1996**, *6*, 15–50.

(40) Kresse, G.; Furthmüller, J. Efficient iterative schemes for ab initio total-energy calculations using a plane-wave basis set. *Phys. Rev. B* **1996**, *54*, 11169–11186.

(41) Blöchl, P. Projector augmented-wave method. *Phys. Rev. B* **1994**, *50*, 17953–17979.

(42) Kresse, G.; Joubert, D. From ultrasoft pseudopotentials to the projector augmented-wave method. *Phys. Rev. B* **1999**, *59*, 1758–1775.

(43) Zones, S.; Van Nostrand, R. Novel zeolite transformations - the template-mediated conversion of cubic-P zeolite to SSZ-13. *Zeolites* **1988**, *8*, 166–174.

(44) Jeanvoine, Y.; Ángyán, J.; Kresse, G.; Hafner, J. Bronsted acid sites in HSAPO-34 and chabazite: An ab initio structural study. *J. Phys. Chem. B* **1998**, *102*, 5573–5580.

(45) Press, W. H.; Flannery, B. P.; Teukolsky, S. A.; Vetterling, W. T. *Numerical Recipes: The Art of Scientific Computing*, 3rd ed.; Cambridge University Press, 2007; p 160.

(46) Bucko, T. Ab initio calculations of free-energy reaction barriers. *J. Phys. Condens. Matt.* **2008**, *20*, 064211.

(47) Himanen, L.; Jäger, M. O.; Morooka, E. V.; Canova, F. F.; Ranawat, Y. S.; Gao, D. Z.; Rinke, P.; Foster, A. S. DScribe: Library of descriptors for machine learning in materials science. *arXiv preprint arXiv:1904.08875* **2019**,

(48) The DScribe libraries are available at https://github.com/SINGROUP/dscribe.

(49) Momma, K.; Izumi, F. *VESTA3* for three-dimensional visualization of crystal, volumetric and morphology data. *J. Appl. Crystallogr.* **2011**, *44*, 1272–1276.

(50) Pohorille, A.; Jarzynski, C.; Chipot, C. Good Practices in Free-Energy Calculations. *J. Phys. Chem. B* **2010**, *114*, 10235–10253.

(51) Chipot, C.; Pohorille, A. In *Free energy calculations: Theory and Applications in Chemistry and Biology*; Chipot, C., Pohorille, A., Eds.; Springer-Verlag Berlin Heidelberg, 2007; pp 40–42.

(52) Valleau, J. P.; Card, D. N. Monte Carlo Estimation of the Free Energy by Multistage Sampling. *J. C. Phys.* **1972**, *57*, 5457–5462.

(53) Lu, N.; Kofke, D. A.; Woolf, T. B. Improving the efficiency and reliability of free energy perturbation calculations using overlap sampling methods. *J. Comput. Chem.* **2004**, *25*, 28–40.

(54) Bennett, C. H. Efficient estimation of free energy differences from Monte Carlo data. *J. Comput. Phys.* **1976**, *22*, 245 – 268.

Table 1: Free energy of activation (eV) computed for the proton exchange reaction in chabazite at T=600 K. The reference free energies for the target methods optPBE-vdW and HSE06 were obtained by a direct MD calculation (Reference A) or through the application of FEPT to 5000 (TS) or 10000 (R) configurations selected from data generated by the production (PBE) method at T=600 K (Reference B). The MLPT results have been obtained as described in Sec. 4.2. The values in parentheses have been determined using the simple overlap sampling (SOS) method as discussed in Sec. 4.5.

	PBE	optPBE-vdW	HSE06
Production/Reference A	0.657	0.752	0.802
Reference B	-	0.749	0.774 (0.798)
MLPT	-	0.751	0.770 (0.797)

Table 2: The performance of the FEPT (without ML), MLPT and MLPT corrected using Eq. 26 (corrected MLPT) methods in predicting the term ΔA_{TS} (see Sec. 2.2) for the transition state of the proton exchange reaction in chabazite at T=600 K. The reported values (eV) for the target method HSE06 have been obtained by averaging over 100 independent random choices of the training set with N_{train} configurations and the values after the $\pm$ sign indicate the corresponding standard deviation. The reference free energies (Reference B) were obtained by a direct application of FEPT to 5000 configurations selected from data generated by the production method at T=600 K.

N_{train}	FEPT	MLPT	corrected MLPT
10	-105.4698± 0.0609	-105.4402± 0.0305	-105.5191± 0.0075
20	-105.4780± 0.0587	-105.4729± 0.0178	-105.5209± 0.0066
50	-105.4926± 0.0438	-105.5017± 0.0090	-105.5184± 0.0068
100	-105.4965± 0.0368	-105.5140± 0.0053	-105.5155± 0.0105
Reference B	-105.5163	-	-

Table 3: Free energy of activation (eV) computed for the proton exchange reaction in chabazite at T=300 K. The reference free energies for the target methods optPBE-vdW and HSE06 were obtained by a direct MD calculation (Reference A) or through the application of FEPT to 5000 (TS) or 10000 (R) configurations selected from data generated by the production (PBE) method at T=300 K (Reference B). The MLPT results have been obtained as described in Sec. 4.3.

	PBE	optPBE-vdW	HSE06
Production/Reference A	0.631	0.707	0.738
Reference B	-	0.727	0.756
MLPT	-	0.728	0.756

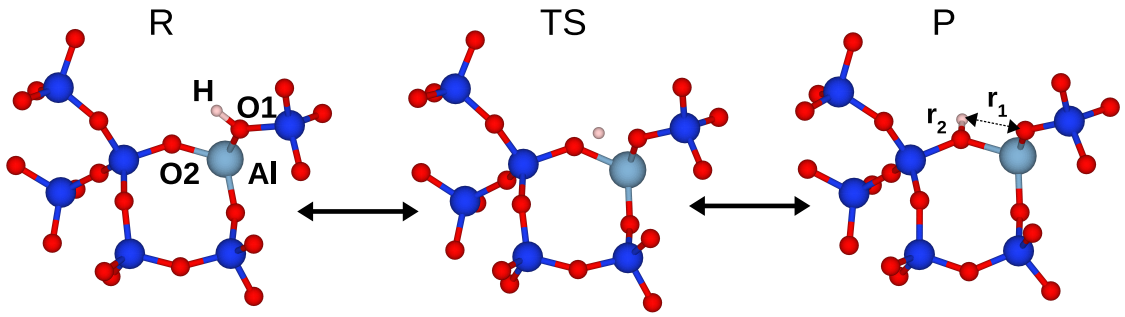

Figure 1: Reactant (R), transition state (TS) and product (P) of the proton exchange between oxygen sites O1 and O2 in zeolite chabazite. The distances between hydrogen and the two oxygen atoms (r_1 and r_2) used in the definition of approximation to reaction coordinate are indicated. The oxygen atoms are labelled according to the nomenclature of Jeanvoine et al.[44]

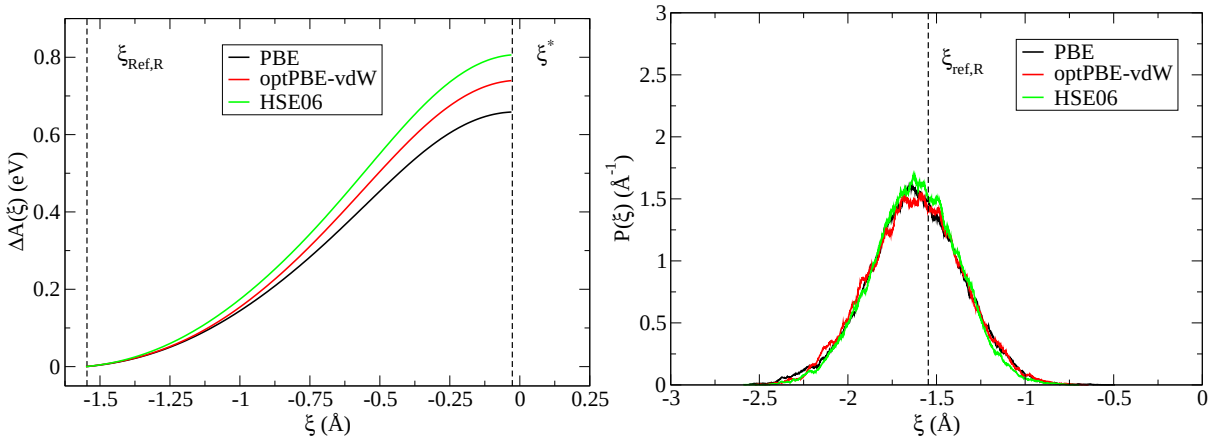

Figure 2: Free energy profiles along the approximation to reaction coordinate (ξ) (left) and the probability distribution functions of ξ (right) determined for the proton exchange reaction in chabazite at 600 K using the PBE, optPBE-vdW, and HSE06 methods. The reference reactant ($\xi_{ref,R}$) and transition (ξ^*) states are indicated by dashed lines.

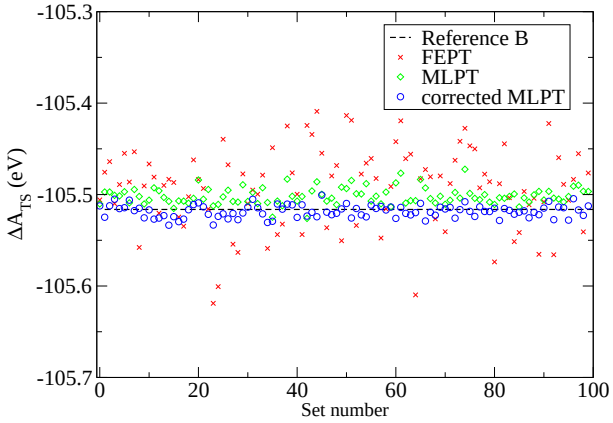

Figure 3: Free energy difference ΔA_{TS} for the proton exchange reaction in chabazite at T=600 K computed using FEPT, MLPT and MLPT corrected using Eq. 26 (corrected MLPT) for the target method HSE06 in 100 independent random choices of the training set with 50 configurations. The reference free energy indicated by the dashed line (Reference B) was obtained by a direct application of FEPT to 5000 configurations selected from data generated by the production method.

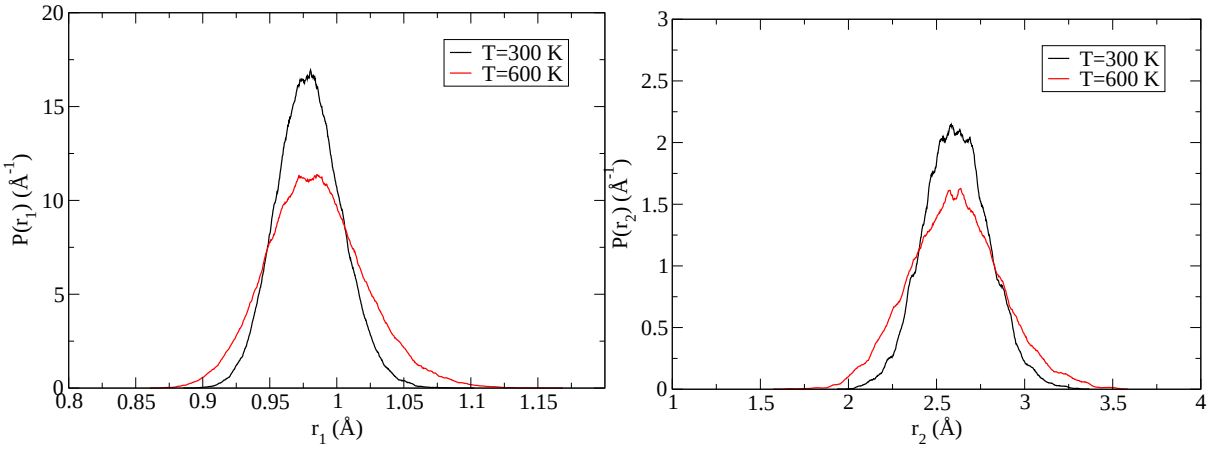

Figure 4: Probability distribution functions of coordinates r_1 (left) and r_2 (right) computed for the reactant state of the proton exchange reaction in chabazite at 300 K and 600 K using MD at the PBE level of theory. In both cases, the low T data form subsets of the high T data.

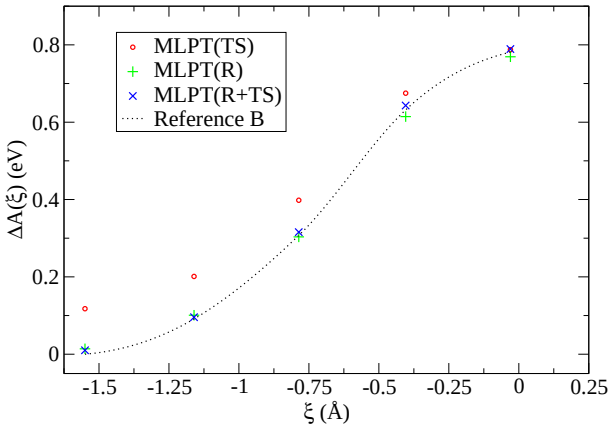

Figure 5: The HSE free energy profile for the proton exchange reaction in chabazite at T=600 K determined using the MLPT method trained on 100 transition state configurations (MLPT(TS)), 100 reactant cofigurations (MLPT(R)), and 50 reactant and 50 transition state configurations (MLPT(R+TS)). The reference free energy profile indicated by the dotted line (Reference B) was obtained by a direct application of FEPT to 5000 configurations of each of 5 intermediate states between $\xi_{Ref,R}$ and ξ^*.

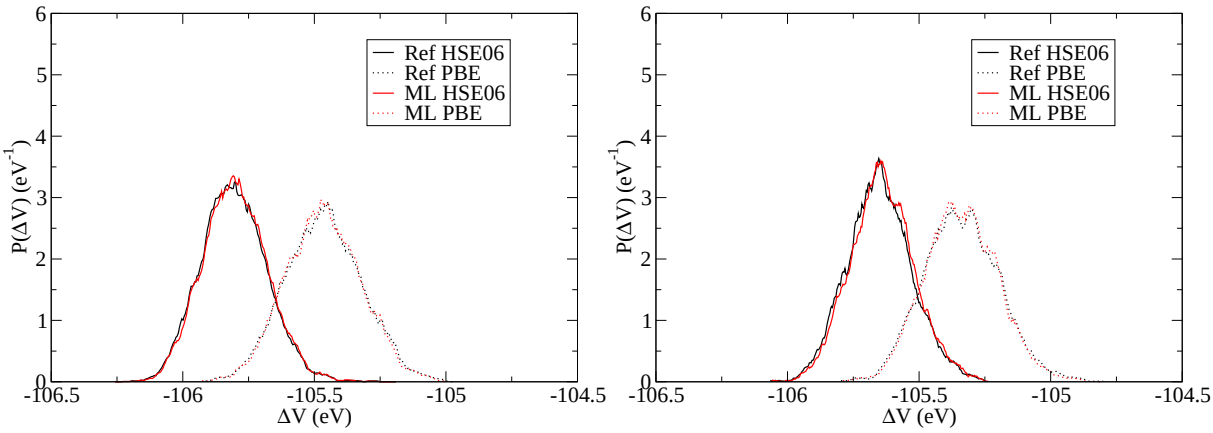

Figure 6: Probability distributions of $\Delta V(\boldsymbol{q})$ computed for PBE production and HSE06 target methods. The distributions are determined using ensembles of structures generated at the HSE06 (full lines) and PBE (dotted lines) levels of theory whereby the $\Delta V(\boldsymbol{q})$ terms were obtained by direct calculation performed for 5000 (TS) or 10000 (R) configurations generated by MD (Ref) or by using the machine learning model trained on 100 configurations generated by MD performed at the PBE level (ML). Results for reactants (left) and transition state (right) configurations are presented.

Graphical TOC Entry